

# We are IntechOpen, the world's leading publisher of Open Access books Built by scientists, for scientists

6,900

Open access books available

186,000

International authors and editors

200M

Downloads

Our authors are among the

154

Countries delivered to

TOP 1%

most cited scientists

12.2%

Contributors from top 500 universities



WEB OF SCIENCE™

Selection of our books indexed in the Book Citation Index  
in Web of Science™ Core Collection (BKCI)

Interested in publishing with us?  
Contact [book.department@intechopen.com](mailto:book.department@intechopen.com)

Numbers displayed above are based on latest data collected.  
For more information visit [www.intechopen.com](http://www.intechopen.com)



---

# Ultrathin Oxide Wrapping of Plasmonic Nanoparticles via Colloidal Electrostatic Self-Assembly and their Enhanced Performances

---

Haoming Bao, Hongwen Zhang,  
Guangqiang Liu and Weiping Cai

Additional information is available at the end of the chapter

<http://dx.doi.org/10.5772/intechopen.79573>

---

## Abstract

Ultrathin and uniform oxide layer-wrapped plasmonic nanoparticles (NPs) have been expected in the fields of light energy conversion and optical sensing fields. In this chapter, we proposed a universal strategy to prepare such core-shell plasmonic NPs based on colloidal electrostatic attraction and self-assembly procedures. Based on the self-assembly strategy, laser ablation of metal targets in liquid medium was conducted at room temperature to one-pot fabricate the oxide-wrapped plasmonic NPs. It demonstrates that a series of core-shell nanostructured NPs such as Au@Fe<sub>2</sub>O<sub>3</sub>, Au@Al<sub>2</sub>O<sub>3</sub>, Au@CuO, Au@ZnO, Pt@TiO<sub>2</sub>, and Pd@TiO<sub>2</sub>, have been readily obtained free of contaminations. Technical analyses illustrate that those composite NPs possess uniform and symmetrical oxides layers with several nanometers in thickness. Furthermore, both the thickness and crystallinity of the oxides layer could be precisely tailored simply by controlling hydrolysis of precursors and irradiation durations. Finally, due to ultrathin wrapping of oxides, the as-obtained core-shell plasmonic NPs show excellent surface-enhanced Raman scattering (SERS) and gas-sensing performances compared with bare metal or oxides NPs.

**Keywords:** plasmonic nanoparticles, ultrathin oxide wrapping, colloidal electrostatic self-assembly, enhanced performances

---

## 1. Introduction

Microstructured/nanostructured plasmonic materials (Au, Ag, Cu, etc.) have great applications in optical sensing [1, 2] and energy conversion [3, 4] due to their surface plasmon-enhanced

---

interaction with incident light. However, in many specific applications, the surfaces of these plasmonic materials need to be modified or coated by organic or inorganic species to achieve core-shell structured nanomaterials with functional properties [5, 6]. Among them, stable semiconducting oxide-coated plasmonic NPs, which couple strong bandgap absorption and plasmon absorption of the light, possess a relatively sensitive surface and have been extremely applied in photo/electro catalysis [7–9], chemical analysis [10, 11], and solar cells [12, 13]. In those applications, the thickness of the shell has been accepted as a fundamental and an important parameter. In particular, the shell is commonly required to be thin enough for maximizing the short-range local surface plasmon resonance (LSPR) effect of the plasmonic metal core. Typically, the wrapping shell thickness is often expected to not exceed 10 nm to ensure strong LSPR effect in the sensitive surface-enhanced Raman scattering (SERS) detection of target analytes [14, 15]. As a result, facile approaches to obtain ultrathin oxides wrapped plasmonic metal NPs are in urgent demands for high performance SERS-based detection application.

In the literature, conventional methods including Stöber method [16], hydrothermal method [17], and sol-gel method [18] have been extremely applied to prepare oxide layers coated plasmonic NPs. For example, Yoshio et al. prepared core-shell structured Ag@SiO<sub>2</sub> NPs through borohydride reduction method [16]. Kim et al. deposited 60 nm of TiO<sub>2</sub> shell layer on gold NPs via microwave-assisted hydrothermal method [17]. In general, these wet chemical fabrications are usually relied on two steps: the formation of the core and subsequent wrapping of the shell, in which an organic substance with multifunctional groups is commonly utilized as a bridge to connect the metal core and the oxide shell. The as-obtained products are often encapsulated with surfactants or the media molecules that cause severe interfering signals in SERS detection and deteriorate the performances in practical applications. What's more, most of these mentioned methods are difficult to achieve ultrathin wrapping layer due to the difficulty in controlling the nucleation and growth stages of the shell. The present reports in literature illustrate that the thickness of the shell is generally thicker than 10 nm, which is beyond or close to the working distance limit of LSPR. And a very few reports regarding one-pot synthesis method could be found for the ultrathin oxides wrapped plasmonic metal NPs [9, 19, 20]. In addition to the wet chemical methods, atomic layer deposition (ALD) has been widely reported to realize homogeneous oxide shell thin to monoatomic layers [21–23]. For example, Qian et al. fabricated Au@TiO<sub>2</sub> core-shell structured NPs by using an electrochemistry controlled atomic layer deposition [22]. However, despite of its ultrathin and uniform oxide shell characters, it is time-consuming and tedious in operation and commonly restricted to deposit Al<sub>2</sub>O<sub>3</sub> or SiO<sub>2</sub> layers. In total, controllable and flexible methods to facilely and one-pot prepare the ultrathin and uniform oxide-coated plasmonic metal NPs free of contaminations are still expected.

Recently, some important progresses have been made in fabrication of ultrathin and uniform oxide-wrapped plasmonic NPs [24, 25]. In this chapter, we introduce a universal strategy for wrapping NPs based on colloidal electrostatic attraction and self-assembly on the plasmonic NPs. Using this strategy and via one-step laser ablation of noble metal targets in the hydrolysis-induced hydroxide sol solutions at room temperature, the oxide shell-wrapped plasmonic NPs with several tens of nanometers in size could be obtained, such as Au@oxides (Fe<sub>2</sub>O<sub>3</sub>, Al<sub>2</sub>O<sub>3</sub>, In<sub>2</sub>O<sub>3</sub>, CuO, and ZnO) as well as Pt@TiO<sub>2</sub> and Pd@TiO<sub>2</sub>.

The oxide shell layers were very uniform and symmetrical and could be controlled from several nanometers down to <1 nm in thickness. The shell thickness shows independence on the plasmonic NPs' size. Finally, the enhanced performances for such oxide layer-wrapped plasmonic NPs were also demonstrated compared with the pure component NPs, mainly including the much stronger SERS performances and the significantly better gas-sensing performance to some toxic molecules.

## 2. Electrostatic Self-Assembly and Laser Ablation in Liquid (LAL) Method

Laser ablation of metal target in colloidal medium will one step produce the nano-sized metal NPs and wrapping of the oxides layer. The physical and chemical properties of oxides shell depend on diverse parameters, including the metal, colloidal type, temperature and pH of the colloidal medium.

### 2.1. Charged properties of colloids

We propose that the surface charge status of both colloids and metal NPs are crucial to the self-assembly formation of oxides shells. Since the surface of the colloids attracts the anions and cations, these ions are distributed in a diffusive state at the two-phase interface to form a diffusion double layer [26–28]. The electric double layer can be divided into two parts by the Stern plane as Stern layer and the diffusion layer. The double layer theory suggests some possible behaviors of the colloids in solution, such as repelling each other and staying stable or attracting each other and coagulating. A parameter quantitatively describes charged properties of the colloids is Zeta potential [27, 28], which refers to the potential of the Shear plane relative to the solution at infinity. The Zeta potential can be positive or negative, which suggests different charged properties of the colloids. The larger the absolute value of Zeta potential usually indicates the more charges on colloids and better stability. If two kinds of colloids charged differently close to each other, a strong electrostatic attraction between them will occur.

### 2.2. Colloidal electrostatic self-assembly

A key issue in the preparation of core-shell-structured NPs is how to efficiently attach the shell materials or its precursors to the preformed core particles. Considering the charging characteristics of colloidal NPs, if two colloidal NPs with different charge properties are brought close to each other, a strong Coulomb attraction will attract them together. When the sizes of the two colloidal NPs differ greatly, the small colloids should be adsorbed onto the surface of the big one to complete the electrostatic assembly process. And such method has been reported for the preparation of Au-wrapped magnetic Fe<sub>3</sub>O<sub>4</sub> NPs [29], and Au-wrapped silica NPs [30]. However, the oxides wrapped plasmonic metal NPs are rarely reported.

In order to achieve the ultrathin oxide wrapping layer, the oxides or its precursor colloids used in the colloidal electrostatic self-assembly should be small enough. Generally, the artificially

assisted methods usually results in bigger oxides or its precursor colloids (most of them are no less than 5 nm). Generally, metal cations ( $\text{Fe}^{3+}$ ,  $\text{Al}^{3+}$ ,  $\text{Cu}^{2+}$ ,  $\text{Ti}^{4+}$ ,  $\text{Sn}^{4+}$ , etc.) are hydrolyzed in solution to form corresponding hydroxide colloids. The size of these hydroxide colloids is generally at several nanometers [31, 32], which is suitable for such a colloidal electrostatic self-assembly. And most of them are positively charged. On the other hand, many plasmonic metal NPs tend to adsorb anions on the surface and carry negative charges [33, 34]. Strong electrostatic attraction between the two kinds of colloids will occur when they are close enough to each other. The small hydroxide colloids will be attached on the surface of the plasmonic metal NPs and a monolayer hydroxide wrapping layer would be formed on the metal NPs due to the colloidal self-assembly, as schematically shown in **Figure 1a** and **b**. After dehydration treatment by annealing or heating, the hydroxides shell will be transformed to corresponding oxides (**Figure 1c**).

Obviously, such a self-assembly process should be a flexible and universal, which is suitable to fabricate a series of core-shell NPs. And the thickness of the shell is highly relied on the size of the colloids produced by the hydrolysis, which could be simply controlled by the pH value and temperature of the colloidal precursor. This has been confirmed by a one-step laser ablation of plasmonic metal target in hydrolyses induced hydroxides sol solutions.

### 2.3. Laser ablation in hydroxides sol solutions

In order to avoid and remove interferences from other substances (such as surfactants), the laser ablation in liquid method, typically been accepted as a chemical green approach, has been adopted to verify the colloidal electrostatic self-assembly strategy.

In the laser-based synthesis procedure, metal foils are usually utilized as the ablation target while metal salt solutions are used as the liquid medium, as shown in **Figure 2**. When a pulsed laser is focused onto the surface of metal target, a localized high-temperature and high-pressure plasma involving atoms, ions, electrons, and clusters is generated. From the moment on formation, the

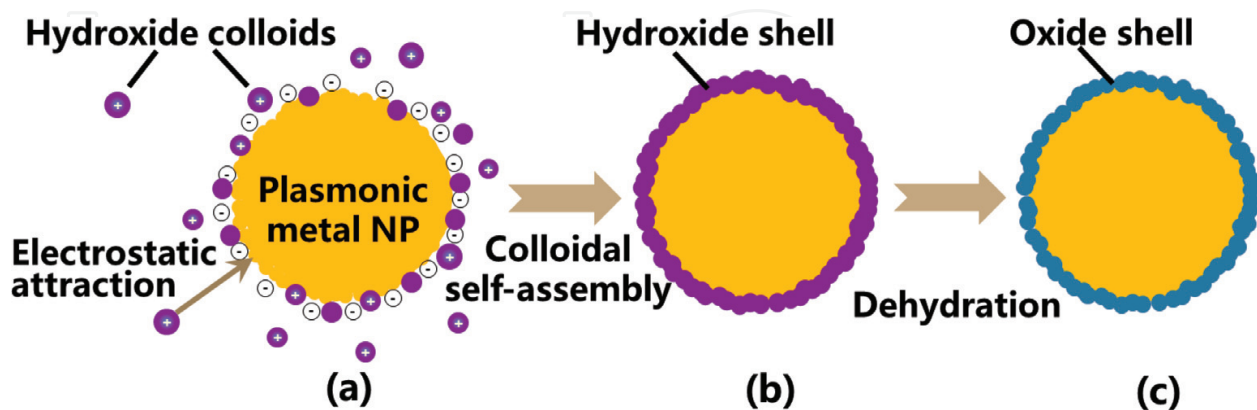


**Figure 1.** Schematic illustration for the fabrication strategy of ultrathin oxide layer-wrapped metal NPs based on the electrostatic colloidal attraction and self-assembly. (a) Adsorption or attachment of hydroxide colloids on a metal NP due to the electrostatic attraction. (b) Formation of monolayer hydroxide colloidal shell by colloidal self-assembly on the metal NP. (c) Formation of ultrathin oxide shell layer on the metal NP by dehydration [24].

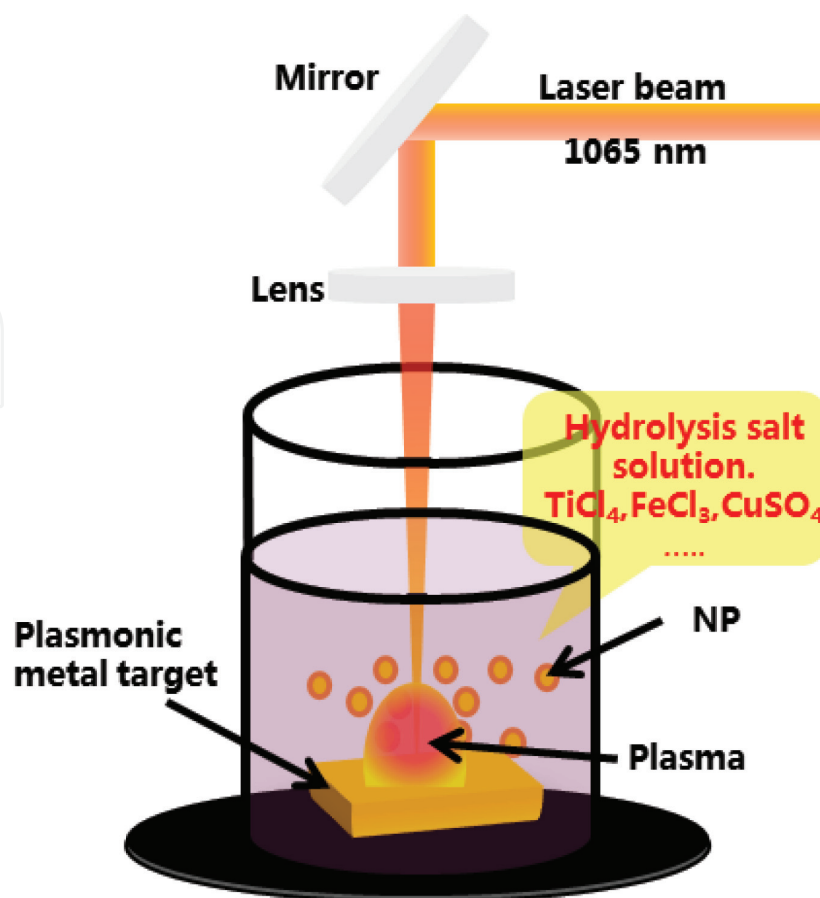


**Figure 2.** Schematic illustration of the laser ablation for ultrathin oxide layer-wrapped plasmonic metal NPs via the colloidal electrostatic self-assembly strategy.

plasma adiabatically expands at supersonic speeds and transfer heat to the surrounding liquid medium. The quenched plasma nucleates and gradually grows up to form plasmonic NPs [35, 36]. Commonly, the newly formed metal NPs are negatively charged and, when they are dispersed into the colloidal solution, they rapidly absorb the cations in the solution. The small hydroxide colloids, which are formed through hydrolysis of the metal cations, in the solution are positively charged. As a result, the metal NPs will electrostatically attract with the positively charged hydroxide colloids. The hydroxide colloids will form a nano-sized layer around the metal core, forming a core-shell structured NP. With the ongoing laser ablation, the hydroxide-based core-shell NPs will absorb the latter arrived laser and slowly dehydrated to oxide shell due to the laser-induced heating.

### 3. LAL-induced oxides wrapped metal NPS

Based on the aforementioned formation process, pulsed laser ablation in colloidal solution will one-pot fabricate the oxides wrapped metal NPs.

### 3.1. Typical morphology and structure of the NPs

First, let us take the  $\text{TiO}_2$ -wrapped Au NPs as an example. The  $\text{Ti}(\text{OH})_4$  sol solution shows obvious Tyndall effect, as shown in the (1–2) of the inset in the **Figure 3a**. The Zeta potential is about +28.9 mV, indicating they are positively charged. And after ablation of a gold target in the sol solution for 15 min, the Zeta potential drops to +26.2 mV, and the pH value was slightly decreased from 1.77 to about 1.65. The Zeta potential of the Au colloidal solution obtained by ablation in pure water was  $-24.2$  mV. After centrifugation for three times of cleaning, the products were redispersed in water to form an aqueous colloidal solution, as shown in inset (3) of **Figure 3a**, and the Zeta potential was almost unchanged and nearly the same as curve (II) in **Figure 3a**. Optical absorption measurement shows that the well-known absorption peak of the Au NPs has an obvious red shift of about 23 nm, which means that the change of the dielectric environment around the Au NPs' surface [7, 37].

**Figure 4** shows the typical microstructure and morphology of the electrostatically assembled core-shell  $\text{Au}@\text{TiO}_2$  NPs. The field emission scanning electron microscope (FESEM) micrographs reveal that the products consist of nearly spherical particles with diameters ranging from 10 to 60 nm with a mean size of 35 nm, as shown in **Figure 4a**. The energy dispersion spectrum (EDS) shows that the product contains the elements of Au, O, Ti, C, and Si, in which Si and C are from the silicon substrate and cleaning reagent, respectively. The inset of **Figure 4b** shows the EDS mapping from a transmission electron microscopy (TEM) of an isolated NP, which reveals that the elements of Ti and O are preferentially distributed on the surface of the spherical Au NP. Corresponding microstructural examination was carried on a TEM (**Figure 4c**), which shows that the surface of these NPs is obviously wrapped with ultrathin (few nanometers) shell layer. The well-defined core-shell structure can be vividly

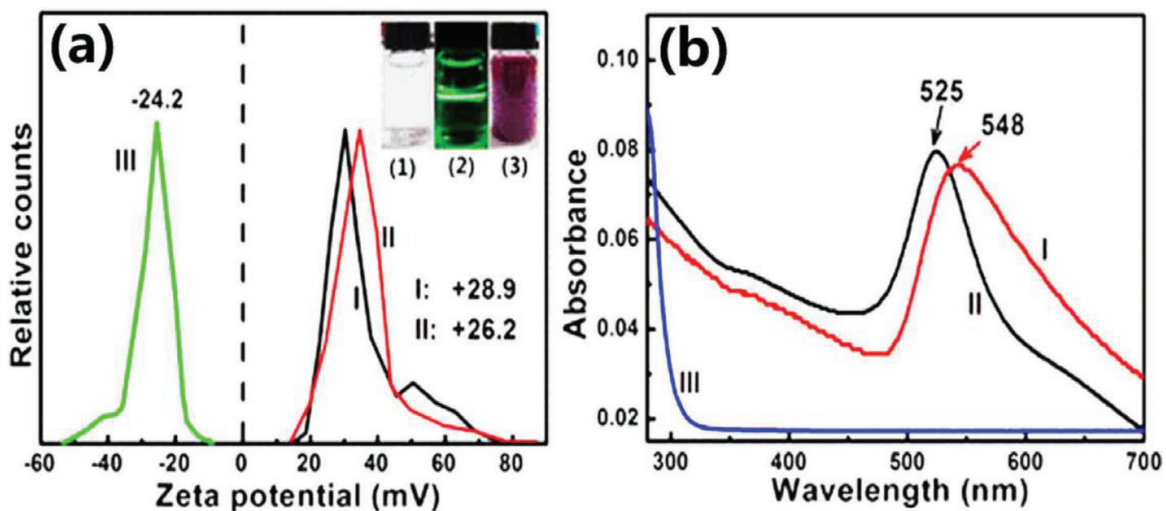


**Figure 3.** (a) Zeta potentials of different colloidal solutions. Curve (I):  $\text{TiCl}_4$  aqueous solution (or  $\text{Ti}(\text{OH})_4$  colloidal solution); Curve (II): the colloidal solution obtained by laser ablation of Au target in the  $\text{TiCl}_4$  aqueous solution without or with centrifugation for cleaning; curve (III): the pure Au colloidal solution induced by laser ablation of Au target in water. The insets (1) and (2) are the photos of the  $\text{Ti}(\text{OH})_4$  colloidal solution without and with an incident laser beam (532 nm), respectively; (3) is the photo of the colloidal solution of curve (II) in (a). (b) Optical absorbance spectra of the different colloidal solutions. Curves (I), (II), and (III) correspond to the samples (II), (III), and (I) in (a), respectively [24].

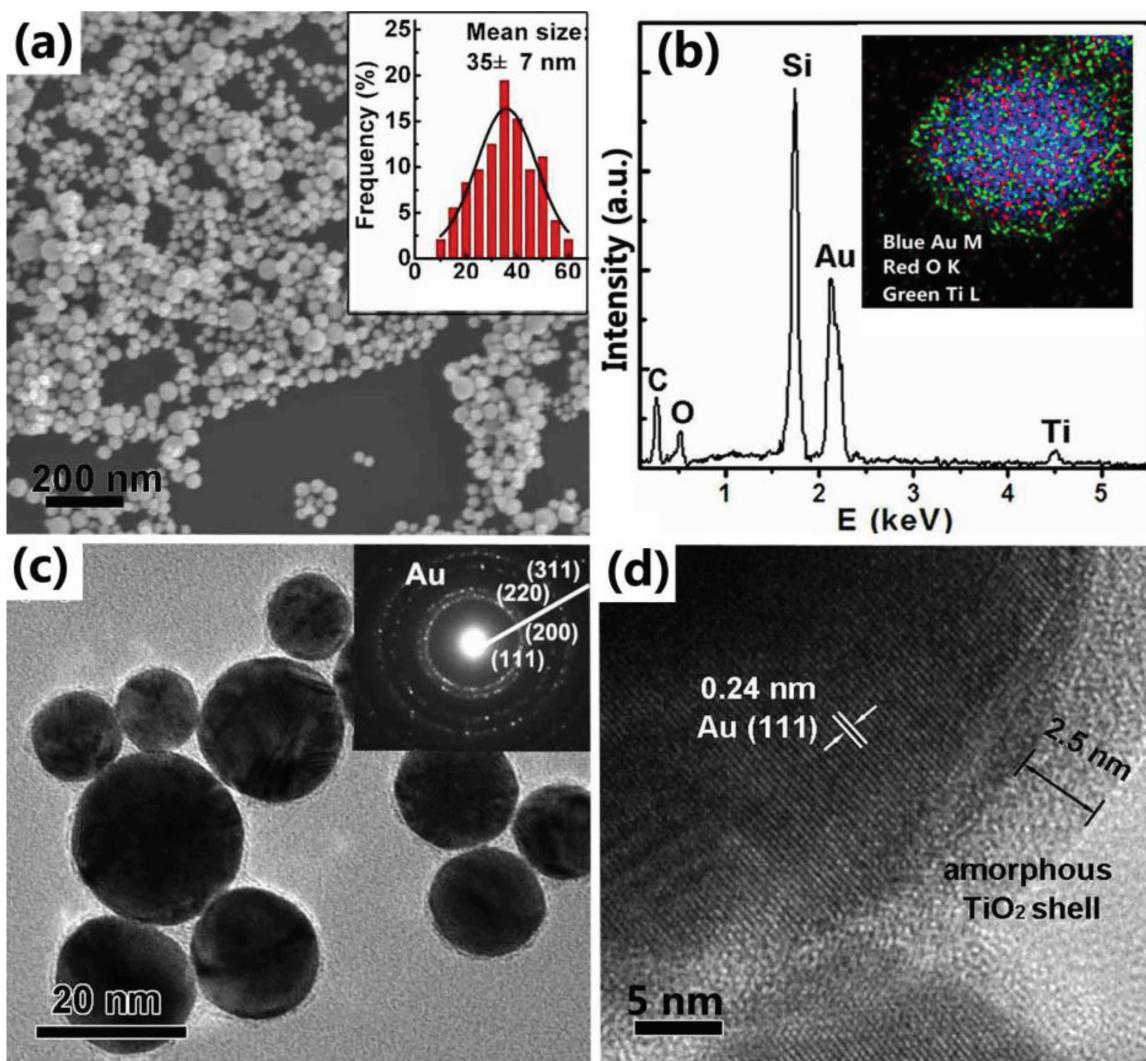


**Figure 4.** Morphological and microstructural observations of the as-prepared products. (a) FESEM image. The inset is the size contribution of the particles. (b) EDS spectrum. The inset is the EDS mapping of a single particle. (c) TEM image. The inset is the corresponding SAED pattern. (d) HRTEM image of a partial particle [24].

observed. However, the corresponding selected area electron diffraction (SAED) pattern only shows the rings of polycrystalline gold, without diffraction pattern belonging to other crystalline substances. High-resolution TEM (HRTEM) photograph (**Figure 4d**) shows clean lattice fringes with an interplanar spacing of 0.24 nm in the core part, which corresponds to the (111) of Au. The shell was measured to be about 2.5 nm in thickness and reveals amorphous nature. Considering the  $\text{Ti}(\text{OH})_4$  precursors in ablation process and existence of Ti and O elements in the wrapping layer, we proposed that the shell might be amorphous  $\text{TiO}_2$ .

In order to further confirm the components of the shell, X-ray diffraction (XRD) measurement was carried out for the products after dropping it on a cleaned amorphous silicon wafer and the subsequent natural drying. There are only three diffraction peaks at  $2\theta = 38.2, 44.4,$  and  $64.6$ , corresponding to crystal planes {111}, {200}, and {220} of the Au crystal with the face-centered cubic structure (PDF, No. 00-001-1172), respectively. No other phase was detected, as illustrated in **Figure 5a**. This confirms the amorphous properties of the shell. The X-ray

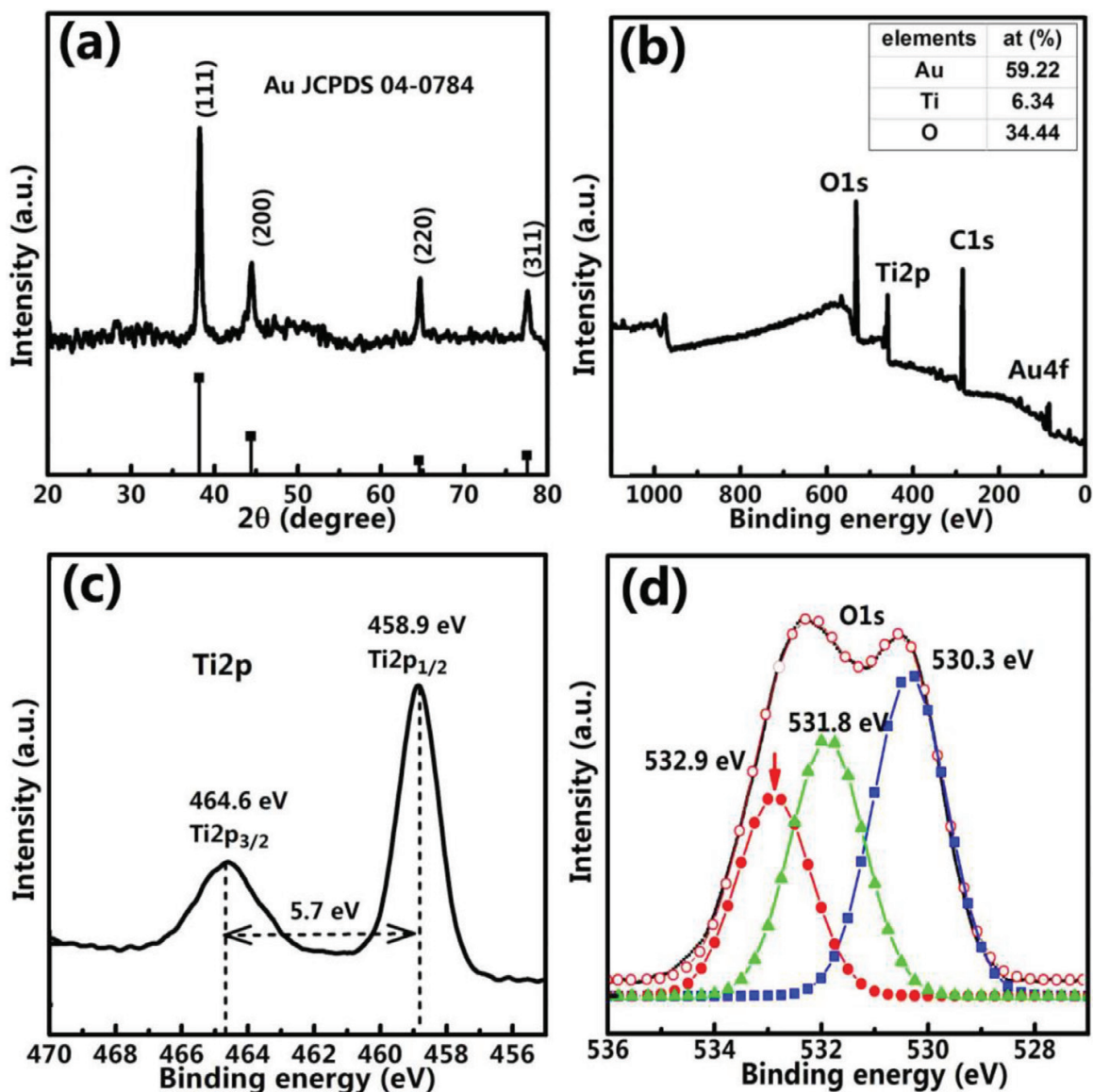


**Figure 5.** (a) XRD pattern of the obtained products. The line spectrum corresponds to the standard pattern of Au powders (JCPDS No. 00-001-1172). XPS spectra of the as-prepared Au@TiO<sub>2</sub> NPs. (b) the full spectrum. (c) Binding energy spectrum of Ti 2p. (d) Binding energy spectrum of O 1s [24].

photoelectron spectrum (XPS) full spectrum presented in **Figure 5b** was also conducted to analyze the surface composition and chemical bonds of the core-shell structured NPs. It shows that the existence of elements Ti, O, and Au. And the atomic ratio of Ti to O is determined to be about 6.34:34.44. The Ti 2p spectrum presented in **Figure 5c** shows two peaks at 464.6 and 458.9 eV correspond to Ti 2p<sub>3/2</sub> and 2p<sub>1/2</sub>, respectively. The splitting with 5.7 eV is in good agreement with the standard value for Ti in TiO<sub>2</sub> [38]. **Figure 5d** presents the spectrum of O 1s, in which strongly overlapping peaks could be found. By a peak differentiation imitating analysis, three peaks at 530.3, 531.8, and 532.9 eV can be parsed out. The peak at 530.3 eV corresponds to the oxygen in TiO<sub>2</sub>, and the peaks at 531.8 and 532.9 eV originate from hydroxyl groups (OH) and adsorbed H<sub>2</sub>O, respectively [38, 39]. Furthermore, the integral area of the peak at 530.3 eV takes 39% of the whole integral area under O 1s spectrum. So the

atomic ratio of Ti to O in the lattice of wrapping layer should be about 6.34: ( $34.44 \times 39\%$ ), or 1:2.1, which is in good agreement with the stoichiometric ratio of  $\text{TiO}_2$ . From the results mentioned previously, the wrapping layer could be confirmed as the amorphous titanium oxide. As an example, it demonstrates that the LAL approach can facily obtain ultrathin oxides wrapped metal NPs.

### 3.2. The universality of LAL fabrication

Furthermore, such LAL synthesis route based on colloidal electrostatic self-assembly has been confirmed as a universal approach, and it is suitable for fabricating many other ultrathin oxide layer-wrapped plasmonic metal NPs, such as  $\text{Au@SnO}_2$ ,  $\text{Au@ZnO}$ ,  $\text{Au@CuO}$ ,  $\text{Au@Al}_2\text{O}_3$ ,  $\text{Au@In}_2\text{O}_3$ , and  $\text{Au@Fe}_2\text{O}_3$  NPs. All the products consist of spherical particles, with about 10–50 nm in mean size. The wrapping layer of these NPs is measured in 2–3 nm [24].

Besides the oxides wrapped Au NPs, the  $\text{Pt@TiO}_2$  and  $\text{Pd@TiO}_2$  NPs can also be prepared via laser ablation in  $\text{Ti(OH)}_4$  sol solution but using the Pt and Pd as ablation targets, respectively. All the core-shell NPs are wrapped with *ca.* 1–3 nm shell layers [24].

It should be pointed out that the method of electrostatic assembly should be suitable for all colloidal systems, only requiring two kinds of colloids with opposite electrical properties and big size gap. Therefore, the plasmonic metal NPs prepared by the traditional wet chemical method can also be wrapped by oxide layers via this strategy.

### 3.3. Confirmation of the electrostatic self-assembly mechanism

The electrostatic self-assembly of colloids has been confirmed by further experiments. First, laser-induced Au NPs from the pure water are slowly (1 mL per min) added into the stirred  $\text{SnCl}_4$  aqueous solution. According to the proposed electrostatic self-assembly mechanism, it should also obtain the ultrathin  $\text{SnO}_2$  layer-wrapped Au NPs, which is confirmed in **Figure 6a**. Similarly, by using the same two-step fabrication, we could also obtain the ultrathin  $\text{TiO}_2$  shell-wrapped Au NPs, as illustrated in **Figure 6b**. The only thing that deserves a bit of attention is that the laser ablation-formed Au NPs should be slowly added into the corresponding hydroxides sol solutions to avoid a possible colloidal coagulation process.

To confirm the opposite charge-induced electrostatic self-assembly mechanism, we ablated Au target in  $\text{Na}_2\text{WO}_4$  solution, which induces both negatively charged Au NPs and  $\text{H}_2\text{WO}_4$  colloids. For this case, no obvious shell can be observed around the Au NPs.

### 3.4. The dependence of the shell thickness

The thickness of the wrapping oxide layer was measured as a function of the Au core's size, as illustrated in **Figure 7**. For the  $\text{Au@TiO}_2$  NPs, the  $\text{TiO}_2$  shell is estimated approximately 2.5 nm in thickness for all NPs regardless of the Au core size. Similarly, the  $\text{SnO}_2$  shell also shows a similar tendency, indicating that the shell is around 2.5 nm for all Au NPs. The shell layer could be the oxides colloidal monolayer formed on Au NPs.

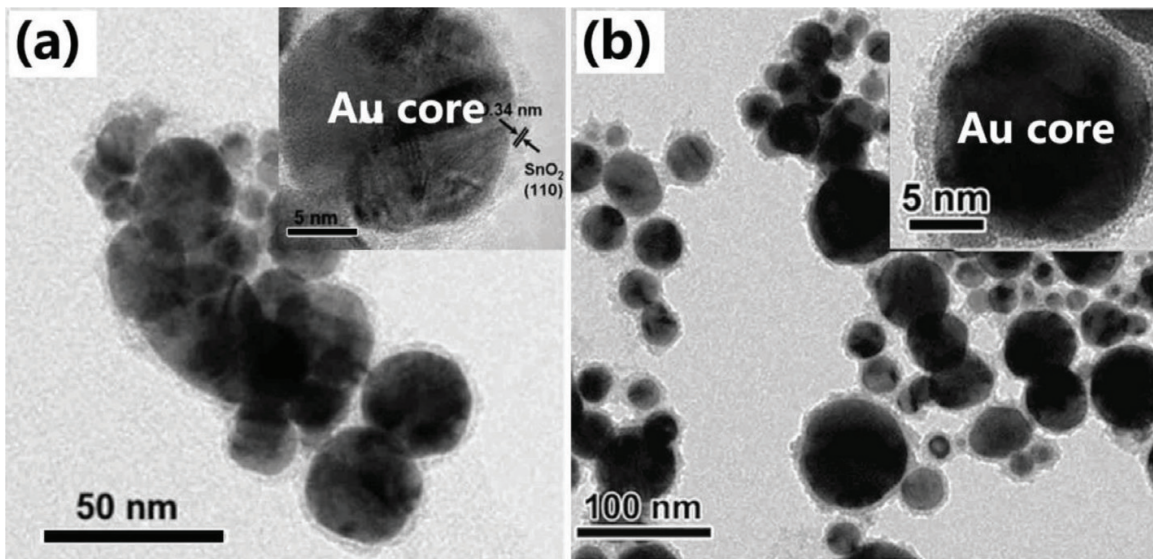


**Figure 6.** TEM image of the products obtained by adding the laser-induced gold colloidal solution into (a)  $\text{Sn}(\text{OH})_4$  and (b)  $\text{Ti}(\text{OH})_4$  sol solution. The inset is the magnified image of a single particle.

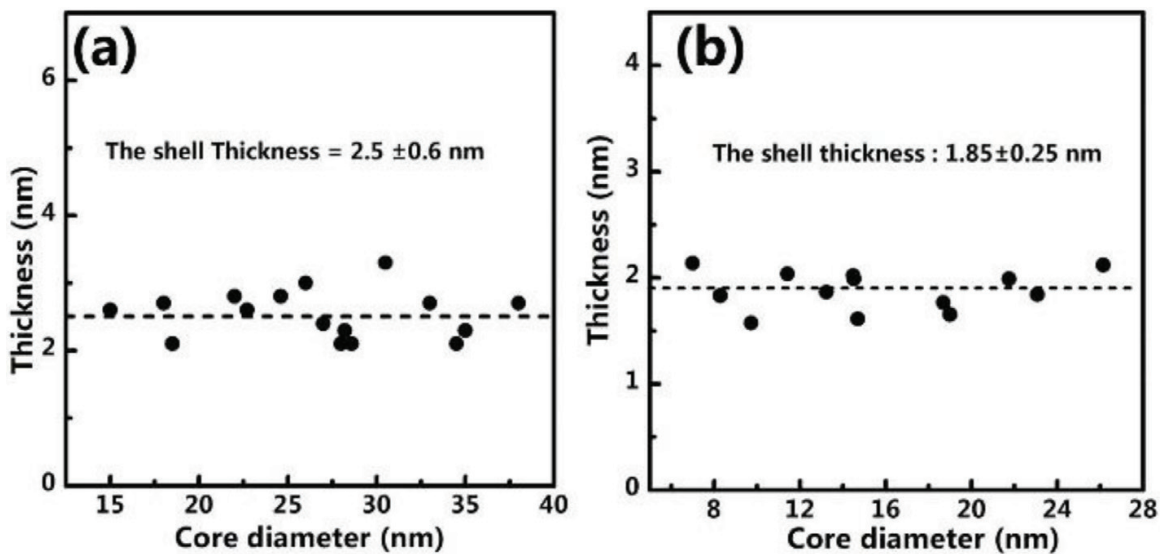


**Figure 7.** Shell thickness versus the core sizes of (a)  $\text{Au}@\text{TiO}_2$  and (b)  $\text{Au}@\text{SnO}_2$  NPs.

### 3.5. The controllability

The laser-based colloidal electrostatic self-assembly strategy shows good flexibility in the fabrication. Here, the controllability in the shell's crystallinity and thickness as well as core's uniformity will be discussed.

#### 3.5.1. Homogenizing the NPs size with secondary irradiation

It is well known that a narrow size distribution is critical to the stable performance of NPs in applications. However, plenty of reports have demonstrated that the laser ablation commonly

lead to formation of NPs with large size distribution. Furthermore, a secondary irradiation technique was proposed as an efficient way to fabricate more uniform NPs. Generally, the gold NPs turn more round and bigger after secondary irradiation treatment [40]. For our Au@SnO<sub>2</sub> NPs, secondary irradiation with wavelength of 532 nm and frequency of 10 Hz for 10 min (yttrium aluminum garnet, and pulse width of 10 ns, 40 mJ per pulse) was also conducted. It has been found that both products show the typical ultrathin wrapped core-shell structure. However, the number of the small NPs is obviously decreased after the secondary irradiation. And this is confirmed by their size distributions. After the secondary irradiation, the distribution becomes narrower and the relative standard deviation (RSD) decreased from 46 to 21%. Additionally, the mean size increased from 12 to 16 nm.

### 3.5.2. The shell crystalline

For some oxides that are easier to crystallize, such as tin oxide, the crystalline shell layer can be usually achieved by a simple drying process. **Figure 8a** and **b** shows TEM and corresponding SAED pattern of the initially prepared Au@SnO<sub>2</sub> NPs. Besides the diffraction rings of Au crystal, some rings of the crystalline SnO<sub>2</sub> also can be observed. The HRTEM image shows the well-defined interplanar spacing of 0.24 and 0.34 nm in the core and shell, corresponding to the (111) and (110) of Au and SnO<sub>2</sub>, respectively. However, for Au@TiO<sub>2</sub> NPs (**Figure 8c** and **d**), most oxides layer is amorphous. Such an amorphous layer may influence or even decrease their performances in optical and electrical applications. Here, we found that the crystallinity of the shell layer could be significantly improved just by prolonging the ablation time. TEM examination has shown that only few areas in the shell layers were crystallized for the sample with 1-h ablation (**Figure 8c**), and for the sample obtained after ablation for 2 h (**Figure 8d**), the shell layers were almost completely crystallized. The lattice fringes with about 0.35 nm in spacing correspond to (101) planes of anatase TiO<sub>2</sub> (PDF, No. 001-0562). Such crystallization

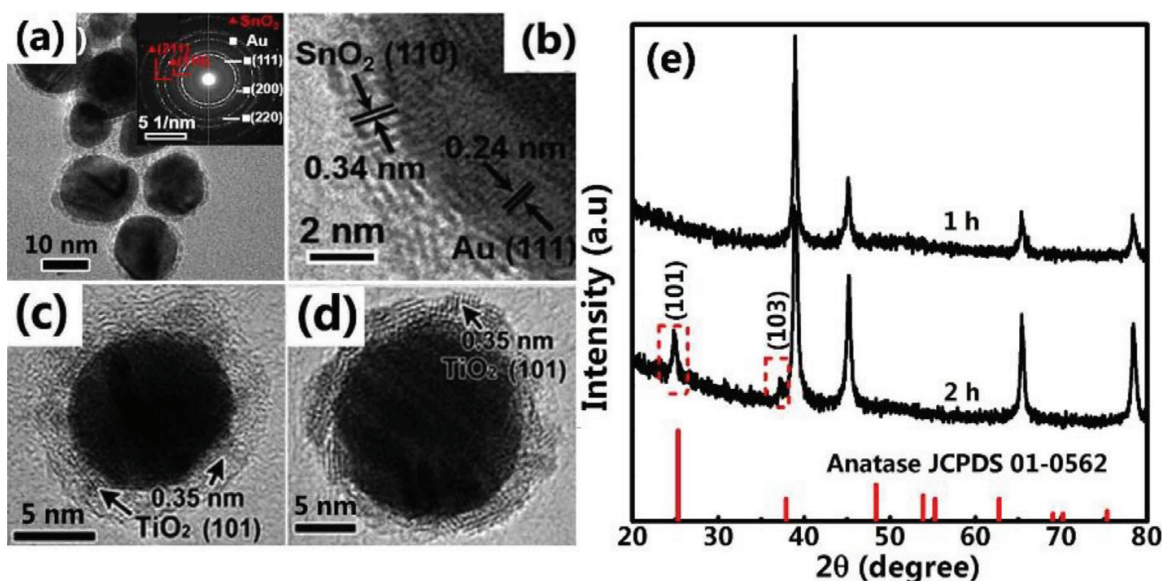


**Figure 8.** (a–d) the TEM observations of the Au@oxides NPs. (a, b) Au NPs wrapped with crystalline SnO<sub>2</sub> shell. (c, d) the Au@TiO<sub>2</sub> NPs prepared by prolonging the laser duration to 1 h (a) and 2 h (b). And (e), the XRD spectra of the Au@TiO<sub>2</sub> NPs corresponding to (c) and (d).

should be attributed to laser-induced thermal effect. The XRD measurements reveal that for products with 1-h ablation, only Au diffraction peaks were detected, while with the ablation duration reached 2-h, additional peaks at 25 and 37° were observed, which correspond to crystal planes (101) and (103) of anatase TiO<sub>2</sub> (**Figure 8e**).

### 3.5.3. The thickness of the shell

Regulation of the wrapping layer thickness for core-shell NPs is a key issue in gas sensing, SERS detection, and catalysis applications. Accordingly, it is critical to realize the flexible regulation of shell thickness. In present colloidal electrostatic self-assembly strategy, we demonstrate that the shell thickness depend only on the size of the hydrolysis-induced hydroxide colloids. As a result, to modulate the wrapping thickness, the hydroxide colloidal size should be precisely controlled by changing experimental parameters such as the concentration, temperature, and pH value of the colloidal solution [41]. Thus, the shell thickness would be simply tuned by changing the related conditions during laser ablation process.

#### 3.5.3.1. The concentrations

If the content of metal ions is too low, most of the Au NPs could not be wrapped with the oxides shell due to insufficient oxide source in the solution. However, if the content of metal ions is too high, the wrapped Au NPs are not obviously increased and even decreased. For example, as illustrated in **Figure 9**, most of the Au@SnO<sub>2</sub> NPs fabricated by ablating Au target in 0.5 M Sn<sup>4+</sup> solution shows that the NPs are fused together. Meanwhile, the wrapping layer thickness is much thinner (approximately 1 nm) than those shown in **Figure 8a** and **b**, and even some NPs are not completely wrapped. In this case, only when the Sn<sup>4+</sup> concentration ranges from 0.01 to 0.1 M, the shell layer of the NPs can be uniform and the Au cores are spherical with nearly same dimensions, as shown in **Figures 8a, b** and **9b**. Although the concentration is difficult to accurately modulate the thickness of the shell, it does obviously affect the thickness of the shell to a certain extent.

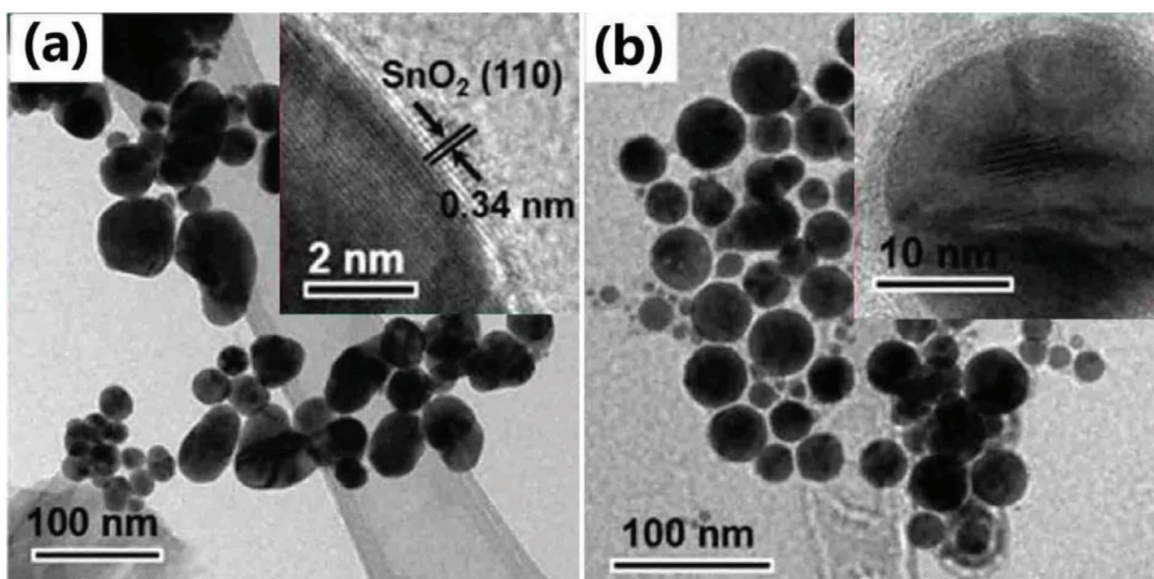


**Figure 9.** TEM observations of the Au@SnO<sub>2</sub> NPs prepared by using 0.5 M (a) and 0.01 M (b) SnCl<sub>4</sub> solutions.

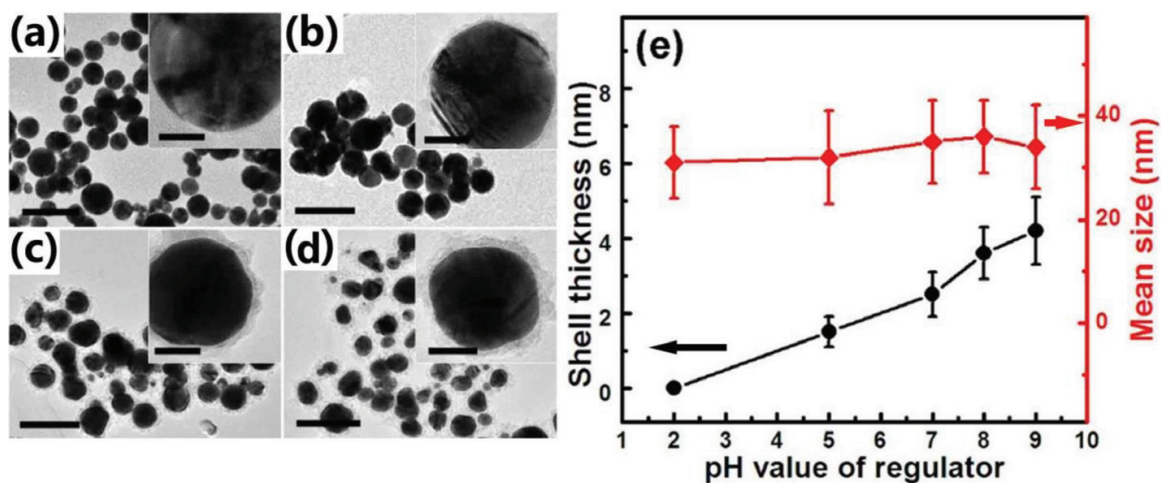


**Figure 10.** The evolution of the shell thickness and size of NPs with the treatment of different pH regulator. (a–d) TEM observations of the NPs obtained with the pH values of 2, 5, 8, and 9, respectively. The scale bars are 50, and 10 nm in the insets. (e) The statistical plots of the shell thickness and mean size versus the pH value of the regulator.

### 3.5.3.2. The temperature

The shell thickness would increase with the temperature increasing of the colloidal solution during laser ablation. Typically, when the temperature of  $\text{Ti}(\text{OH})_4$  sol solution was increased to  $50^\circ\text{C}$ , the mean thickness was about 3.8 nm. If the temperature was increased up to  $95^\circ\text{C}$ , the shell was about 5.5 nm in thickness.

### 3.5.3.3. The pH value

Furthermore, the pH value of precursor solution also dramatically influences the shell thickness. By simply dropping regulator solution (NaOH or HCl solution) in the laser ablation process with a dropping rate of  $10 \mu\text{L}$  per min,  $\text{Au}@\text{TiO}_2$  NPs with diverse shell thicknesses are achieved. **Figure 10a–d** shows typical TEM photographs of isolated nanoparticles obtained under different pH regulators. It is worth noting that when the pH of the regulator is too low (pH = 2), the oxide shell disappears (**Figure 10a**). And with the pH increase, the shell thickness increases obviously. However, the sizes of Au NPs have no obvious changes (30–35 nm, red line in **Figure 10e**).

## 4. Enhanced performance

### 4.1. High performance SERS detection

As mentioned previously, ultrathin oxide layer–wrapped plasmonic metal NPs have potential applications in many fields. Among them, SERS substrate, which consisted of the core-shell NPs, has huge applications in the detection of some special target molecules that are difficult to be efficiently detected by pure plasmonic metal substrate due to their weak interaction.

#### 4.1.1. SERS effect of the oxide-wrapped plasmonic metal NPs

Due to the strong LSPR effect of gold cores, strong local electromagnetic field thus can be formed near the surface of the NPs with the incident light irradiating. It is reasonable that such core-shell NPs illustrate SERS effect to specific target molecules. However, considering that the SERS is a short-range effect, the distance it can effectively act on is generally considered not to exceed 10 nm on the plasmonic particle surface. As previously reported [15], the enhancement effect of SERS decreases exponentially with the shell thickness increasing. So, the SERS activity of the coated Au NPs should be much lower than that of pure Au NPs due to the existence of the wrapping layer.

#### 4.1.2. Enhanced interaction between analytes and SERS substrate

Improvement of the interaction between the analytes and the SERS substrates is important in SERS-based detection. For the analytes which weakly interact with plasmonic metal NPs but can strongly be adsorbed on oxides, the ultrathin oxide layer-wrapped plasmonic metal NPs could be the better SERS substrate than the pure noble metal NPs.

For example, the explosive raw material  $\text{KNO}_3$ , which weakly interacts with the Au NPs, was utilized as the analyte. Because of the positively charged  $\text{Au@TiO}_2$  NPs in  $\text{KNO}_3$  solution, the surface of NPs could enrich more nitrate anions than the pure negatively charged Au NPs. Thus, the  $\text{Au@TiO}_2$  NPs-built film as the SERS substrate can adsorb the molecules well for further SERS detection. **Figure 11a** presents the Raman spectra for the  $\text{Au@TiO}_2$  NPs and the pure Au NPs substrates after soaking in the  $\text{KNO}_3$  solution with 1000 ppm and drying. For the  $\text{Au@TiO}_2$  NPs substrate, there exists a strong main peak at  $1048 \text{ cm}^{-1}$  together with a relatively weak peak at  $712 \text{ cm}^{-1}$  and a very weak peak at  $1345 \text{ cm}^{-1}$ . Such a spectral pattern is in good agreement with that of pure solid  $\text{KNO}_3$ , and

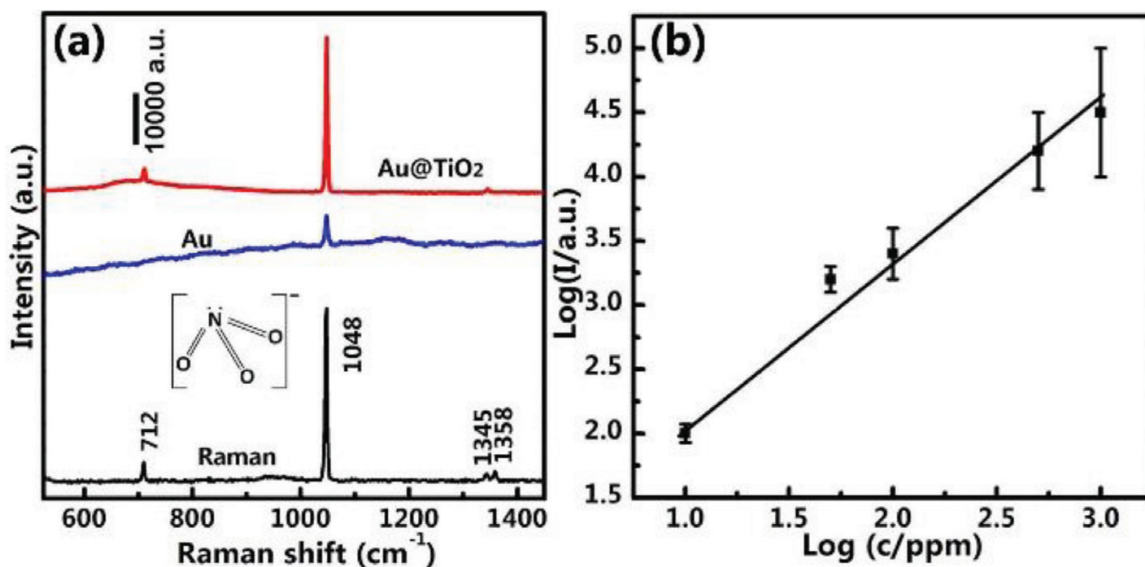


**Figure 11.** (a) Raman spectra of  $\text{KNO}_3$  on different substrates of  $\text{Au@TiO}_2$  NPs and pure Au NPs, respectively, after soaking in the  $\text{KNO}_3$  solution with 1000 ppm. And the Raman spectrum of pure solid  $\text{KNO}_3$ . (b) Plot of the peak intensity  $I$  at  $1048 \text{ cm}^{-1}$  versus the  $\text{KNO}_3$  concentration  $C$  for the soaked  $\text{Au@TiO}_2$  substrate [24].

all the peaks should originate from nitrate  $\text{NO}_3^-$  [42]. In contrast, the signal from the Au NP-built substrate was much lower. The intensity of the main peak at  $1048\text{ cm}^{-1}$  is five times higher for the Au@TiO<sub>2</sub> substrate than that from the Au NPs' substrate. Furthermore, the Raman spectral dependence on the  $\text{NO}_3^-$  concentration was measured for the Au@TiO<sub>2</sub> substrate, as demonstrated in **Figure 11b**. It shows the plot of the peak intensity at  $1048\text{ cm}^{-1}$  versus the  $\text{NO}_3^-$  concentration, which exhibits a good linear double logarithmic relation between them. The SERS detection limit is less than 1 ppm.

#### 4.1.3. Reusability of SERS substrate

Most SERS substrates are often disposable. As a result, the reusability of them is significantly important from the view of economics and complexity in the repeated fabrication of substrate. As we known, the oxides have shown excellent photocatalyst properties in many previous works. The oxide wrapping layer is thus expected to photocatalyze the target molecules after a SERS detection. Indeed, the reusability of the Au@TiO<sub>2</sub> NP substrate has been confirmed, as previously reported [24]. Typically, the 4-Nitrophenol (4-NP), which can be photocatalyzed by TiO<sub>2</sub>, [43] was used as the target molecules for SERS detection. The Raman spectrum of the Au@TiO<sub>2</sub> NP-built film after soaking in the 4-NP solution with 20 ppm is well shown. All Raman peaks are from 4-NP molecules [44]. If the soaked film was subsequently irradiated for 5 min by a xenon lamp before Raman spectral measurement, the Raman signals are significantly decreased. A 10-min irradiation led to complete disappearance of the Raman peaks. After re-soaking the substrate in the 4-NP solution before Raman measurement, we can obtain the Raman spectrum with the similar peak intensities to those of the initial one, showing good reusability of Au@TiO<sub>2</sub> NPs for the SERS-based detection of such molecules.

## 4.2. Enhanced gas sensing

It is well known that metal oxides are typical gas-sensing materials and are sensitive to many gas molecules such as NO<sub>2</sub>, NH<sub>3</sub>, H<sub>2</sub>S, etc., exhibiting huge application prospect in this field. Here, the colloidal electrostatic self-assembly formed oxides wrapped gold NPs also has shown excellent performance in the gas sensing.

#### 4.2.1. Fast response at room temperature

Usually, the significant responses to the gas molecules generally occur at a high temperature (200–450°C). Thus, the response to gas molecules at room temperature is very important due to low power consumption and safety purpose (especially for some inflammable gases). It has been found that such colloidal electrostatic self-assembly formed Au@SnO<sub>2</sub> NPs are much better in the gas sensing to H<sub>2</sub>S gas at room temperature than the pure SnO<sub>2</sub> NPs' film [45].

Typically, the responses to H<sub>2</sub>S gas (1–3 ppm) at room temperature for these two NPs build films are illustrated in **Figure 12a**. For the pure SnO<sub>2</sub> NPs' film, the response to H<sub>2</sub>S at room temperature was not recoverable [25]. As a result, the pure SnO<sub>2</sub> NPs' film cannot be used at room temperature for detection of H<sub>2</sub>S gas. While for Au@SnO<sub>2</sub> sensor, the response was quickly recovered to the baseline upon gas off. Besides, Au@SnO<sub>2</sub> exhibits much faster

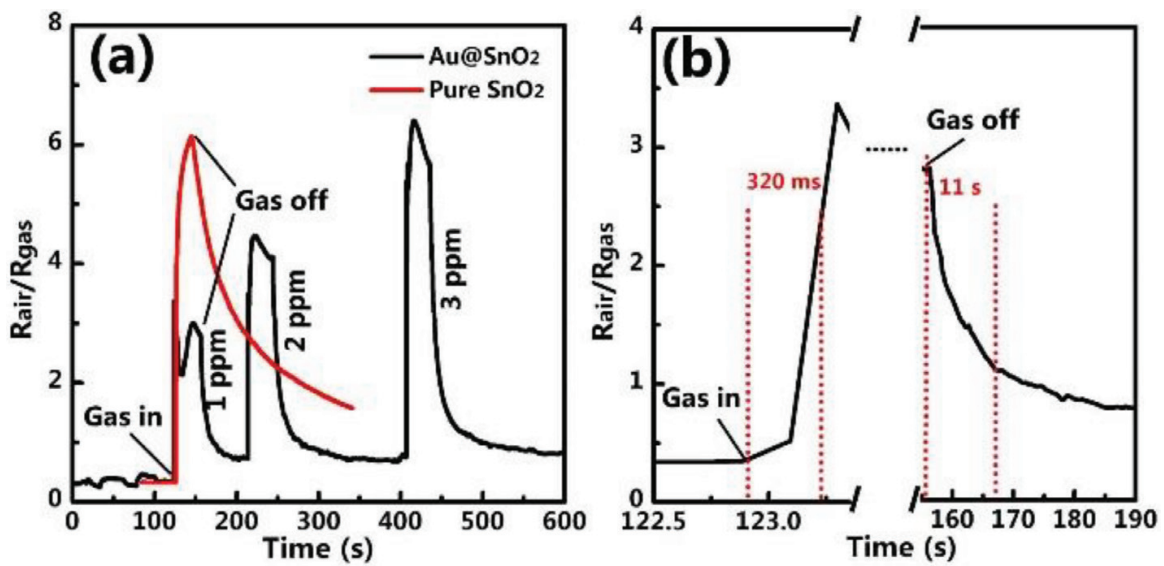


**Figure 12.** (a) Responses to H<sub>2</sub>S gas at room temperature for the Au@SnO<sub>2</sub> NPs' film and the pure SnO<sub>2</sub> NPs' film. (b) The response and recover part of the plot of Au@SnO<sub>2</sub> NPs' film to 1 ppm H<sub>2</sub>S gas.

response (320 ms) and recovery (11 s) compared with pure SnO<sub>2</sub> counterpart (**Figure 12b**). This could be associated with both electronic sensitization of Au metal and the ultrathin wrapping layer in such a core/shell structure. Further work is needed to understand and reveal the origin of this phenomenon.

#### 4.2.2. Quantifiable sensing and selectivity

Quantitative detection makes sensing more reliable and scientific. The response of Au@SnO<sub>2</sub> NPs to H<sub>2</sub>S here shows obvious concentration dependence. With the concentration increasing from 1 to 10 ppm, the sensitivity increases linearly, as shown in **Figure 13a**. This provides an

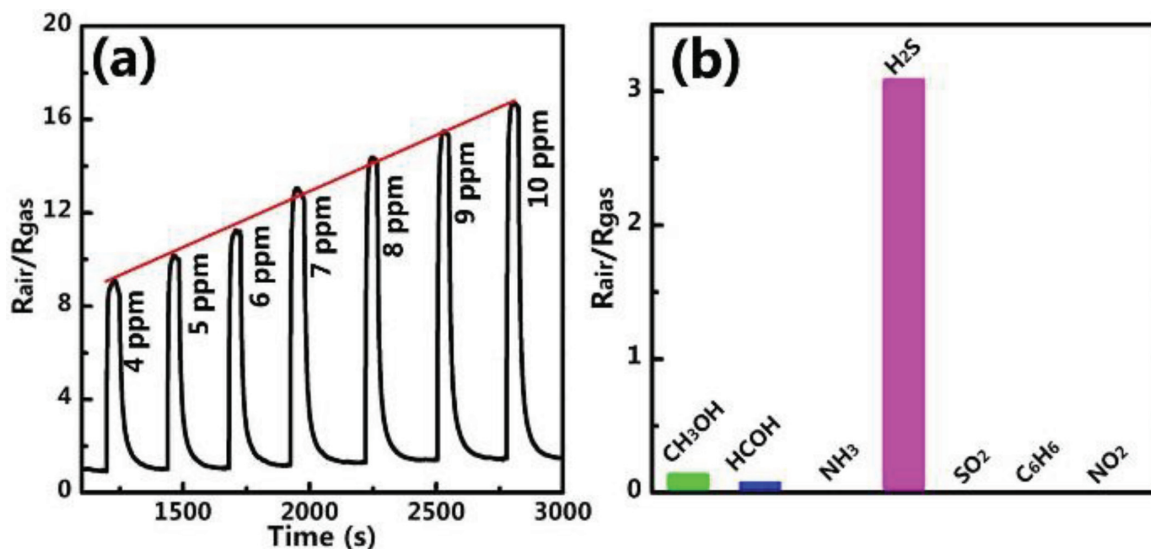


**Figure 13.** (a) The responses of the Au@SnO<sub>2</sub> NPs' film to different concentrations of H<sub>2</sub>S gas. (b) The selectivity of the substrates to a variety of gases.

opportunity for the quantitative gas detection of H<sub>2</sub>S at room temperature. In addition, such core-shell materials also show good selectivity to the H<sub>2</sub>S gas. Under the same test conditions and gas concentration, it shows no responses to a variety of gases, such as ammonia and benzene vapor, and only shows weak responses to alcohol and formaldehyde vapors. And the corresponding sensitivity was 24 and 38 times lower than that of substrate to H<sub>2</sub>S gas, as shown in **Figure 13b**.

In short, since many metal oxides can be used as the gas-sensing materials, the colloidal electrostatic self-assembly fabrication can provide a general method to achieve the ultrathin metal layer-wrapped plasmonic NPs, which are a class of new gas-sensing materials.

## 5. A brief summary

We have introduced a facile strategy for fabrication of ultrathin oxide layer-wrapped plasmonic metal NPs based on colloidal electrostatic attraction and self-assembly. In this approach, hydrolysis-induced small positively charged hydroxide colloids are wrapped on negatively charged plasmonic metal NPs via the electrostatic self-assembly. After dehydration process by annealing, the shell will be transformed to oxide, resulting in oxides wrapped metal NPs. Based on this strategy, one-step laser ablation of metal targets in the hydrolysis-induced hydroxide sol solutions have been conducted to fabricate the Au@oxides (Fe<sub>2</sub>O<sub>3</sub>, Al<sub>2</sub>O<sub>3</sub>, Al<sub>2</sub>O<sub>3</sub>, CuO, and ZnO) as well as Pt@TiO<sub>2</sub> and Pd@TiO<sub>2</sub> NPs. Furthermore, the thickness of these oxide layers are as thin as 1~3 nm and homogenous. And it also shows independence on the plasmonic metal NPs' size. Additionally, such a strategy shows excellent controllability to the shell in the fabrication. Typically, a secondary irradiation can homogenize the NPs' size. Prolonging the ablation duration can improve the shell's crystallinity hugely. And the shell thickness also could be tuned by the temperature, concentration, and pH value, simply by adjusting the hydrolysis of the metal ion. Finally, enhanced SERS and gas-sensing performances of such oxide layer-wrapped plasmonic metal NPs also have been demonstrated. It demonstrates that ultrathin TiO<sub>2</sub>-wrapped Au NPs can achieve a much stronger SERS performances in the detection of nitrates due to its positively charged composite NPs. In addition, such a SERS substrate can be recycled by irradiating the used substrate to photodegrade the target organic molecules. Also, significantly better gas-sensing performance of Au@SnO<sub>2</sub> NPs has been studied, which demonstrates quickly and linearly respond to H<sub>2</sub>S gas at room temperature with excellent selectivity.

## Acknowledgements

This work is financially supported by the National Key Research and Development Program of China (Grant No. 2017YFA0207101), Natural Science Foundation of China (Grant Nos. 51771182, 51531006, and 11574313), and the CAS/SAF International Partnership Program for Creative Research Teams.

## Author details

Haoming Bao<sup>1,2</sup>, Hongwen Zhang<sup>1\*</sup>, Guangqiang Liu<sup>1</sup> and Weiping Cai<sup>1,2\*</sup>

\*Address all correspondence to: hwzhang@issp.ac.cn; wpcai@issp.ac.cn

1 Key Laboratory of Materials Physics, Anhui Key Laboratory of Nanomaterials and Nanotechnology, Institute of Solid State Physics, Chinese Academy of Sciences, Hefei, PR China

2 University of Science and Technology of China, Hefei, PR China

## References

- [1] Homola J, Yee SS, Gauglitz G. Surface plasmon resonance sensors: Review. *Sensors and Actuators B*. 1999;**54**(1–2):3-15
- [2] Homola J. Surface plasmon resonance based sensors. *Analytical and Bioanalytical Chemistry*. 2006;**377**(3):528-539
- [3] Devi BP, Wu KC, Pei Z. Gold nanomesh induced surface plasmon for photocurrent enhancement in a polymer solar cell. *Solar Energy Materials & Solar Cells*. 2011;**95**(8): 2102-2106
- [4] Barazzouk S, Hotchandani S. Enhanced charge separation in chlorophyll a solar cell by gold nanoparticles. *Journal of Applied Physics*. 2004;**96**(12):7744-7746
- [5] Liu B et al. Influence of dimensionality and crystallization on visible-light hydrogen production of Au@TiO<sub>2</sub> core-shell photocatalysts based on localized surface plasmon resonance. *Catalysis Science & Technology*. 2018;**8**(4):1094-1103
- [6] Kim M et al. Efficient visible light-induced H<sub>2</sub> production by Au@CdS/TiO<sub>2</sub> nanofibers: Synergistic effect of core-shell structured Au@CdS and densely packed TiO<sub>2</sub> nanoparticles. *Applied Catalysis B: Environmental*. 2015;**s166–167**(10):423-431
- [7] Sun Y et al. Complete Au@ZnO core-shell nanoparticles with enhanced plasmonic absorption enabling significantly improved photocatalysis. *Nanoscale*. 2016;**8**(20):10774-10782
- [8] Kuo CH et al. Facet-dependent and Au nanocrystal-enhanced electrical and photocatalytic properties of Au–Cu<sub>2</sub>O core-shell heterostructures. *Journal of the American Chemical Society*. 2011;**133**(4):1052-1057
- [9] Han L et al. One-pot synthesis of a Au@TiO<sub>2</sub> core-shell nanocomposite and its catalytic property. *RSC Advances*. 2013;**3**(31):12568-12570
- [10] Lin XD et al. Synthesis of ultrathin and compact Au@MnO. *Journal of Raman Spectroscopy*. 2012;**43**:40-45

- [11] Chen L et al. SERS study of surface plasmon resonance induced carrier movement in Au@Cu<sub>2</sub>O core-shell nanoparticles. *Spectrochimica Acta Part A: Molecular and Biomolecular Spectroscopy*. 2018;**189**:608-612
- [12] Liu WL et al. The influence of shell thickness of Au@TiO<sub>2</sub> core-shell nanoparticles on the plasmonic enhancement effect in dye-sensitized solar cells. *Nanoscale*. 2013;**5**(17):7953
- [13] Fan R et al. Tailored Au@TiO<sub>2</sub> nanostructures for plasmonic effect in planar perovskite solar cells. *Journal of Materials Chemistry A*. 2017;**5**(24):12034-12042
- [14] Moskovits M. Surface-enhanced spectroscopy. *Reviews of Modern Physics*. 1985;**57**(3):783-826
- [15] Li JF et al. Shell-isolated nanoparticle-enhanced Raman spectroscopy. *Nature*. 2010;**1267**(1):392-395
- [16] Kobayashi Y et al. Silica coating of silver nanoparticles using a modified Stöber method. *Journal of Colloid and Interface Science*. 2005;**283**(2):392-396
- [17] Kim YS, Rai P, Yu YT. Microwave assisted hydrothermal synthesis of Au@TiO<sub>2</sub> core-shell nanoparticles for high temperature CO sensing applications. *Sensors and Actuators B: Chemical*. 2013;**186**(6):633-639
- [18] Chung FC, Wu RJ, Cheng FC. Fabrication of a Au@SnO<sub>2</sub> core-shell structure for gaseous formaldehyde sensing at room temperature. *Sensors and Actuators B: Chemical*. 2014;**190** (Complete):1-7
- [19] Solovyeva VA et al. One-pot synthesis of Au@SiO<sub>2</sub> catalysts: A click chemistry approach. *ACS Combinatorial Science*. 2014;**16**(10):513
- [20] Pastorizas I et al. One-pot synthesis of Ag@TiO<sub>2</sub> core-shell nanoparticles and their layer-by-layer assembly. *Langmuir*. 2000;**16**(6):2731-2735
- [21] Kikuchi K et al. Room temperature atomic layer deposition of TiO<sub>2</sub> on gold nanoparticles. *Journal of Vacuum Science & Technology A*. 2017;**35**(1):01B121-(1-5)
- [22] Qian L et al. Widely tuning optical properties of nanoporous gold-titania core-shells. *Journal of Chemical Physics*. 2011;**134**(1):014707
- [23] Bai Y et al. Core-shell Si@TiO<sub>2</sub> nanosphere anode by atomic layer deposition for Li-ion batteries. *Journal of Power Sources*. 2016;**308**:75-82
- [24] Bao H et al. Ultrathin oxide layer-wrapped noble metal nanoparticles via colloidal electrostatic self-assembly for efficient and reusable SERS substrates. *Langmuir*. 2017;**33**:12934-12942
- [25] Bao H et al. Ultrathin tin oxide layer-wrapped gold nanoparticles induced by laser ablation in solutions and their enhanced performances. *Journal of Colloid and Interface Science*. 2017;**489**:92-99
- [26] Verwey E, Overbeek J, Nes KV, Theory of the Stability of Lyophobic Colloids: The Interaction of Sol Particles Having an Electric Double Layer. Amsterdam: Elsevier, 1948

- [27] Hunter RJ, et al. Interaction Between Colloidal Particles—Zeta Potential in Colloid Science—Appendix 5. Zeta Potential in Colloid Science. San Diego: Academic Press; 1981, pp. 363-369
- [28] Hunter RJ, Ottewill RH, Rowell RL. Zeta Potential in Colloid Science. San Diego: Academic Press; 1981, pp. 11-58
- [29] Liu G et al. Electrostatic self-assembly of Au nanoparticles onto thermosensitive magnetic core-shell microgels for thermally tunable and magnetically recyclable catalysis. *Small*. 2015;**11**(23):2807-2816
- [30] Sadtler B, Wei A. Spherical ensembles of gold nanoparticles on silica: Electrostatic and size effects. *Chemical Communications*. 2002;**15**(15):1604
- [31] Liu Z et al. Adhesion of *Escherichia coli* and *Bacillus subtilis* to amorphous Fe and Al hydroxides and their effects on the surface charges of the hydroxides. *Journal of Soils and Sediments*. 2015;**15**(11):2293-2303
- [32] Brodskii VA et al. Electro-surface properties of metal oxides and hydroxides in water solutions. *Glass and Ceramics*. 2015;**72**(5–6):220-224
- [33] Perito B et al. Antibacterial activity of silver nanoparticles obtained by pulsed laser ablation in pure water and in chloride solution. *Beilstein Journal of Nanotechnology*. 2016;**7**(1): 465-473
- [34] Nikov RG et al. Stability of contamination-free gold and silver nanoparticles produced by nanosecond laser ablation of solid targets in water. *Applied Surface Science*. 2012;**258**(23): 9318-9322
- [35] Simakin AV et al. Nanoparticles produced by laser ablation of solids in liquid environment. *Applied Physics A*. 2004;**79**(4–6):1127-1132
- [36] Patil PP et al. Pulsed-laser-induced reactive quenching at liquid-solid interface: Aqueous oxidation of iron. *Physical Review Letters*. 1987;**58**(3):238
- [37] Zhang L et al. Geometry control and optical tunability of metal-cuprous oxide core-shell nanoparticles. *ACS Nano*. 2012;**6**(4):3514-3527
- [38] Zhang H et al. Defect-mediated formation of Ag cluster-doped TiO<sub>2</sub> nanoparticles for efficient photodegradation of pentachlorophenol. *Langmuir*. 2012;**28**(8):3938-3944
- [39] Gole A et al. Pepsin–gold colloid conjugates: Preparation, characterization, and enzymatic activity. *Langmuir*. 2001;**17**(5):1674-1679
- [40] Wang H et al. Selective pulsed heating for the synthesis of semiconductor and metal submicrometer spheres. *Angewandte Chemie International Edition*. 2010;**49**(36):6361-6364
- [41] Surender GD, et al. Synthesis of ultrafine rutile phase titanium dioxide particles. US. 2008. Patent No. 7,413,726. Washington, DC: U.S

- [42] Shi YE, Wang W, Zhan J. A positively charged silver nanowire membrane for rapid on-site swabbing extraction and detection of trace inorganic explosives using a portable Raman spectrometer. *Nano Research*. 2016;**9**(8):2487-2497
- [43] Marcì G et al. Influence of tungsten oxide on structural and surface properties of sol-gel prepared TiO<sub>2</sub> employed for 4-nitrophenol photodegradation. *Journal of the Chemical Society, Faraday Transactions*. 1996;**92**(5):819-829
- [44] Muniz-Miranda M. SERS monitoring of the catalytic reduction of 4-nitrophenol on Ag-doped titania nanoparticles. *Applied Catalysis B: Environmental*. 2014;**146**(3):147-150
- [45] Tans SJ, Verschueren ARM, Dekker C. Room-temperature transistor based on single carbon nanotube. *Nature*. 1997;**393**:49-52

IntechOpen

